The Extended Hadamard Transform

How does open access to this work benefit you?
Let us know @ library@weizmann.ac.il

(article begins on next page)

The Extended Hadamard Transform: Sensitivity-Enhanced NMR Experiments Among Labile and Non-Labile [1]Hs of SARS-CoV-2-derived RNAs

Dr. Jihyun Kim[1], Dr. Mihajlo Novakovic[1], Prof. Dr. Sundaresan Jayanthi[2], Dr. Adonis Lupulescu[3], Dr. Ēriks Kupče[4], Dr. J. Tassilo Grün[1], Ms. Klara Mertinkus[5], Mr. Andreas Oxenfarth[5], Prof. Dr. Harald Schwalbe[5], and Prof. Dr. Lucio Frydman[1*]

[1]Department of Chemical and Biological Physics, Weizmann Institute of Science, Rehovot 7610001, Israel

[2]Department of Physics, Indian Institute of Space Science and Technology, Valiamala, Thiruvananthapuram 695 547, Kerala, India

[3]"Horia Hulubei" National Institute for Physics and Nuclear Engineering IFIN-HH, 30 Reactorului Street, 077125 Bucharest-Măgurele, Romania

[4]Bruker UK, Banner Lane, Coventry, UK

[5]Institute of Organic Chemistry and Chemical Biology, Center for Biomolecular Magnetic Resonance, Johann Wolfgang Goethe-University, D-60438 Frankfurt/Main, Germany

Abstract

Hadamard encoded saturation transfer can significantly improve the efficiency of NOE-based NMR correlations from labile protons in proteins, glycans and RNAs, increasing the sensitivity of cross-peaks by an order of magnitude and shortening experimental times by ≥100-fold. These schemes, however, fail when tackling correlations *within* a pool of labile protons –for instance imino-imino correlations in RNAs or amide-amide correlations in proteins. Here we analyze the origin of the artifacts appearing in these experiments, and propose a way to obtain artifact-free correlations both within the labile pool as well as between labile and non-labile [1]Hs, while still enjoying the gains arising from Hadamard encoding and solvent repolarizations. The principles required for implementing what we define as the extended Hadamard scheme are derived, and its clean, artifact-free, sensitivity-enhancing performance is demonstrated on RNA fragments derived from the SARS-CoV-2 genome. Sensitivity gains per unit time approaching an order of magnitude are then achieved in both imino-imino and imino-amino/aromatic protons 2D correlations; similar artifact-free sensitivity gains can be observed when carrying out extended Hadamard encodings of 3D NOESY/HSQC-type experiments. The resulting spectra reveal significantly more correlations than their conventionally acquired counterparts, which can support the spectral assignment and secondary structure determination of structured RNA elements.

---

[*] To whom correspondence should be addressed: lucio.frydman@weizmann.ac.il

Introduction

Multidimensional NMR correlations play an essential role in structural and dynamic elucidations of organic and biological molecules.[1,2] These correlations occur when the polarization is transferred among spins via stochastic processes like chemical exchange or the nuclear Overhauser effect (NOEs),[3–6] or through coherent J-couplings as in Total Correlation SpectroscopY (TOCSY)[7,8] or heteronuclear (HSQC, HMQC) correlations.[9,10] However, detecting these transfers –particularly homonuclear NOESY cross-peaks– can often be challenged by the relatively low efficiencies of the polarization transfers. This limitation becomes even more acute when detecting cross-peaks involving labile protons. In these cases, inter-site correlations involving the labile protons can be lost by chemical exchanges with the solvent, resulting in weak or no cross-peaks to/from such sites. To alleviate this problem measurements on hydroxyl, amino, imino or even amide protons often need to be performed at low temperatures where solvent exchanges occur more slowly, or signal averaged over long periods of time. Neither of these options is optimal for studying complex biomolecules under physiological conditions.

We have recently demonstrated a number of avenues whereby solvent exchanges can be used to enhance correlations involving labile protons.[11–14] For instance, instead of a single t_1 encoding followed by a mixing time, the peaks of interest can be encoded and cross-correlated by looping multiple encoding / mixing times.[11] During each mixing time, labile protons are then repolarized through exchange processes with an unperturbed water ^1H magnetization, acting as a source for a more efficient polarization transfer. As a result, a sensitivity enhancement is imparted on cross-peaks between labile and non-labile sites, facilitating 2D NOESY and TOCSY correlations. Alternatively, one can target the labile peaks of interest one-by-one, with a frequency-selective irradiation. If carried out with continuous irradiations this may be considered as a special case of the selective looped manipulations, as labile repolarizations by solvent exchanges will occur continuously rather than discretely during the inter-loop delays, leading for instance to selective magnetization transfer (SMT) experiments.[14] Although lacking Fourier multiplexing these experiments can, in analogy to Saturation Transfer Experiments (STD),[15] deliver NOE cross-peaks showing an enhanced sensitivity compared to conventional methods. Further enhancements of such correlations can be achieved by incorporating into SMT a Hadamard scheme,[16–18] whereby monochromatic frequency-selective pulses are replaced by polychromatic saturation or polychromatic inversion pulse blocks, perturbing multiple labile peaks in what will become

the F_1 frequency domain. As this perturbation is encoded with a Hadamard matrix, pure correlations from each peak are revealed by a suitable Hadamard reconstruction of the data. By replacing the t_1 time-domain Fourier encoding with a Hadamard frequency-domain encoding, the efficiency of the 2D NMR measurement on a sparse system is remarkably increased: in favorable cases, the ensuing the Hadamard magnetization transfer (HMT) scheme can lead to NOE cross-peaks whose signal-to-noise (SNR) per unit time is enhanced by over two orders of magnitude, compared to their conventionally-collected counterparts.

HMT and NOEs: The Problem of Intra-group correlations

Despite the advantages of HMT, the method has a major drawback: it only works reliably when used to correlate nuclei comprising spectrally distinct spin pools. This was illustrated in ref. [14], which showed that although HMT could provide reliable cross-peaks between different spin pools, it will in general fail when connectivities are sought within the same pool of spins –e.g., when seeking imino-imino correlations within nucleic acids. This problem originates from Hadamard assumption of a linear independence between the weightings imparted to the various peaks during its frequency encoding. In other words, Hadamard encoding assumes that when addressing multiple sites, the effects imparted by the RF on the signal of one site, will not interact with the effects it imparts on another site. This can be more clearly appreciated if considering a basic four-site, four-scans scenario, involving a Hadamard-based saturation of the sites. In such scenario, the Hadamard-encoded experiment will be defined by a 4x4 matrix $\{c_{lm}\}$, where $1 \leq m \leq n_p$ indexes the various peaks, and $1 \leq l \leq n_S$ indexes the various scans. We write the elements of such matrix as

Scan l \ Peak m	A	B	C	D
I	-1	-1	-1	-1
II	1	1	-1	-1
III	-1	1	1	-1
IV	1	-1	1	-1

where -1 means saturation of a given peak m in scan l; +1 means no saturation (note that the +1 and -1 in the Hadamard matrix do not indicate states of magnetization). If no site cross-relaxes with any of the other sites being irradiated, it is straightforward to evaluate the outcome of each measurement: no peaks will be detected in experiment I, peaks A and B will arise in measurement II, and so on. That is

Scan l \ Peak m	A	B	C	D
I	/	/	/	/
II	A	B	/	/
III	/	B	C	/
IV	A	/	C	/

To decode the contribution from individual sites a Hadamard reconstruction is then applied, involving summations according to the columns employed in the encoding of the sites. That is: the contribution from each site will arise from combining the signals $\{S_l\}$ in experiments $1 \leq l \leq 4$, weighted by the ± 1 coefficients in the columns of the $\{c_{lm}\}$ matrix. For instance

$$(-I + II - III + IV) \rightarrow (-\{0 + 0 + 0 + 0\} + \{A + B + 0 + 0\} - \{0 + B + C + 0\} + \{A + 0 + C + 0\}) = 2A.$$

$$(-I + II + III - IV) \rightarrow (-\{0 + 0 + 0 + 0\} + \{A + B + 0 + 0\} + \{0 + B + C + 0\} - \{A + 0 + C + 0\}) = 2B \tag{1}$$

and so on. Notice the factor of 2 in front of each site, corresponding to the $\sqrt{\#scans}$ enhancement that Hadamard multiplexing brings on top of a site-by-site irradiation of the kind happening in SMT.

Consider now the situation that arises if setting up the same Hadamard scheme, but among mutually cross-relaxing sites. For example, assume a situation where sites A, B and C cross-relax with one another, while site D does not cross-relax with any other sites. The execution of the Hadamard-encoded experiment described above, will then lead to

Scan l \ Peak m	A	B	C	D
I	/	/	/	/
II	$A - \Delta A_C$	$B - \Delta B_C$	/	/
III	/	$B - \Delta B_A$	$C - \Delta C_A$	/
IV	$A - \Delta A_B$	/	$C - \Delta C_B$	/

where the red arrows denote the cross-relaxing sites, and the ΔX_Y terms represent a cross-relaxation into site X arising because of the saturation of site Y. The same Hadamard reconstruction procedure mentioned earlier, will now lead to:

A: $(-I + II - III + IV) \rightarrow (-\{0 + 0 + 0 + 0\} + \{A - \Delta A_C + B - \Delta B_C + 0 + 0\} - \{0 + B - \Delta B_A + C - \Delta C_A + 0\} + \{A - \Delta A_B + 0 + C - \Delta C_B + 0\}) = \mathbf{2A} - \Delta \mathbf{A_B} - \Delta \mathbf{A_C} + \Delta \mathbf{B_A} - \Delta \mathbf{B_C} + \Delta \mathbf{C_A} - \Delta \mathbf{C_B}$

B: $(-I + II + III - IV) \rightarrow (-\{0 + 0 + 0 + 0\} + \{A - \Delta A_C + B - \Delta B_C + 0 + 0\} +$
$\{0 + B - \Delta B_A + C - \Delta C_A + 0\} - \{A - \Delta A_B + 0 + C - \Delta C_B + 0\}) = \mathbf{2B} - \Delta B_A - \Delta B_C +$
$\Delta A_B - \color{red}{\Delta A_C} + \Delta C_B - \color{red}{\Delta C_A}$ (2)

and so on. Notice that this is not what one would want, as the actual NOE spectrum should only exhibit contributions from the directly cross-relaxing sites; i.e.,

A: $\mathbf{2A} - 2\Delta A_B - 2\Delta A_C + 2\Delta B_A + 2\Delta C_A$

B: $\mathbf{2B} - 2\Delta B_A - 2\Delta B_C + 2\Delta A_B + 2\Delta C_B$ (3)

etc. The terms highlighted in red in Eq. (2) –also shown in Figure 1– are therefore artifacts arising from cross-talks between the saturated sites. Notice that such artifacts only arise from Hadamard encoding when more than one proton within a cross-relaxing proton network is perturbed (i.e. saturated or inverted) per scan; no artifacts arise in SMT, as in this experiment sites are addressed one by one.[14] As mentioned, however, SMT will not be as efficient as an ideal HMT, which enjoys the advantages of both solvent repolarization effects and of a Hadamard multiplexing.
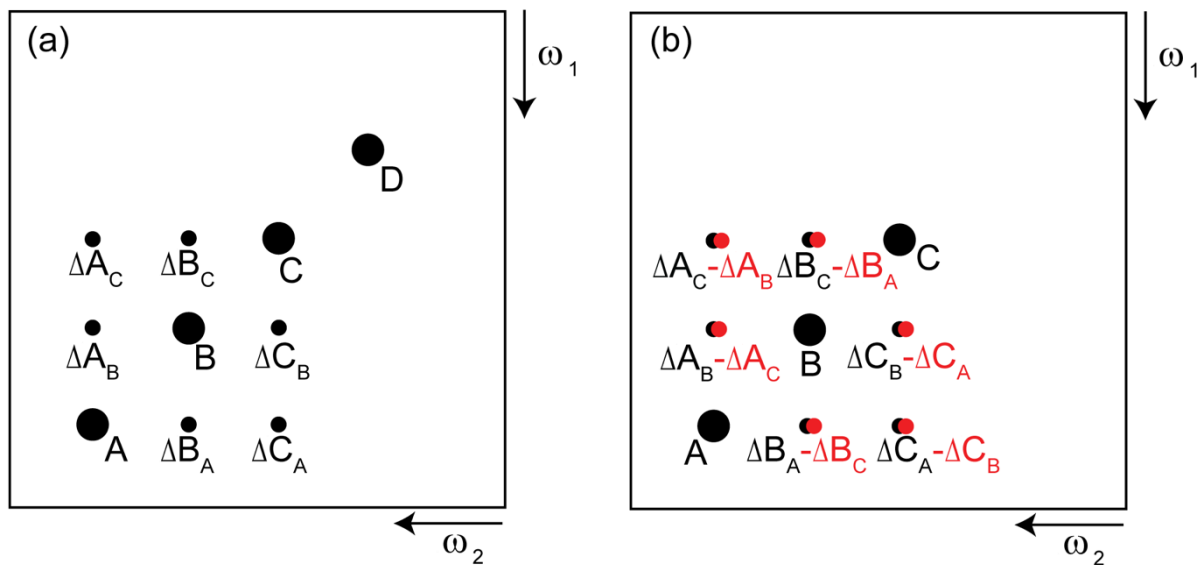

Figure 1. Schematic differences between: (a) An ideal 2D NOESY spectrum containing diagonal peaks (big circles marked A, B, C, D), and genuine contributions from cross-relaxing sites (small circles marked by Δs). (b) The spectrum obtained from a reconstruction based on an HMT encoding. Depending on the cross-relaxation between A, B and C, the latter can provide cross-peak contributions marked in red, that do not involve the pairs of sites being correlated. These contributions can be positive, zero, or negative, and while generally smaller than the real cross-peaks between the two targeted sites, their magnitudes cannot be ascertained or disentangled from the latter.

In addition to the continuous saturation approach just analyzed, the Hadamard encoding scheme was also demonstrated on the basis of selective, polychromatic

inversions.[12] As in the continuous saturation irradiation case, this inversion-based strategy will involve selective pulses applied at the frequencies of the peaks to be encoded, changing from scan to scan on the basis of a Hadamard encoding. In order to enjoy from the solvent-exchange enhancements arising in the saturation experiments this pulsed inversion approach is repeated a number of times, with a mixing time introduced between inversions so as to fully replenish the original labile ^{1}H polarization via exchanges with the water ^{1}Hs (Figure 2a). It is enlightening to consider whether such inversion-based experiments will also suffer from the above-mentioned artifacts. To do so, we assume again a four-site system, with sites A, B and C cross-relaxing with each other, subject to the aforementioned $\{c_{lm}\}_{1 \leq m \leq n_p, 1 \leq l \leq n_S}$ Hadamard encoding matrix. In this case, however, $c_{lm} = -1$ will mean an inversion and $+1$ means no inversion. The spectral traces that will arise after the Hadamard reconstruction, will then be

Peak m / Scan l	A	B	C	D
I	$-A$	$-B$	$-C$	$-D$
II	$A - 2\Delta A_C$	$B - 2\Delta B_C$	$-C + 2\Delta C_A + 2\Delta C_B$	$-D$
III	$-A + 2\Delta A_B + 2\Delta A_C$	$B - 2\Delta B_A$	$C - 2\Delta C_A$	$-D$
IV	$A - 2\Delta A_B$	$-B + 2\Delta B_A + 2\Delta B_C$	$C - 2\Delta C_B$	$-D$

A Hadamard reconstruction procedure will now lead to:

A: $(-I + II - III + IV) \rightarrow (-\{-A - B - C - D\} + \{A - 2\Delta A_C + B - 2\Delta B_C - C + 2\Delta C_A + 2\Delta C_B - D\} - \{-A + 2\Delta A_B + 2\Delta A_c + B - 2\Delta B_A + C - 2\Delta C_A - D\} + \{A - 2\Delta A_B - B + 2\Delta B_A + 2\Delta B_C + C - 2\Delta C_B - D\}) = \mathbf{4A - 4\Delta A_B - 4\Delta A_C + 4\Delta B_A + 4\Delta C_A}$

B: $(-I + II + III - IV) \rightarrow (-\{-A - B - C - D\} + \{A - 2\Delta A_C + B - 2\Delta B_C - C + 2\Delta C_A + 2\Delta C_B - D\} + \{-A + 2\Delta A_B + 2\Delta A_c + B - 2\Delta B_A + C - 2\Delta C_A - D\} - \{A - 2\Delta A_B - B + 2\Delta B_A + 2\Delta B_C + C - 2\Delta C_B - D\}) = \mathbf{4B - 4\Delta B_A - 4\Delta B_C + 4\Delta A_B + 4\Delta C_B}$ (4)

and so on. Notice that in such pulsed inversion experiments (i) sensitivity is doubled vis-à-vis the saturation version as a result of taking differences between positive and negative peaks (instead of between positive and zeroed ones), and (ii) one can now obtain artifact-free cross-peaks from all resonances.
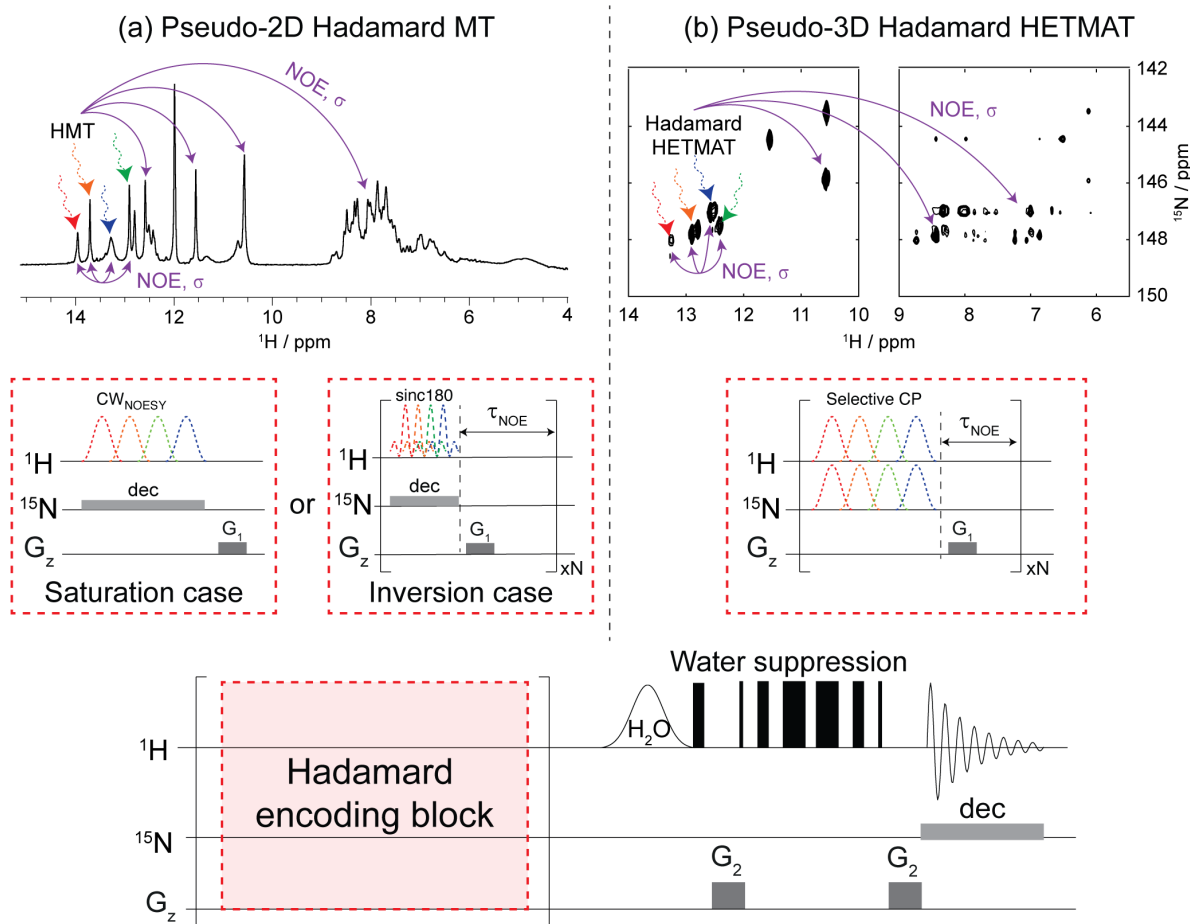
Figure 2. Hadamard-encoded (or extended Hadamard-encoded) pulse sequences for (a) Magnetization Transfer (MT) and (b) HETeronuclear MAgnetization Transfer (HETMAT) experiments. The first row illustrates how peaks of interest –in this case assumed to be iminos in nucleic acids– are selected, and what correlations are detected in each experiment. In MT imino protons are selected and Hadamard-encoded by selective polychromatic saturations, or by looped polychromatic inversions; in HETMAT looped Hadamard-encoded selective cross-polarization (CP) modules are applied (red dashed boxes). Note that as in HETMAT the imino peaks are selected based on the frequencies of both the ^{15}N and the ^{1}H, pseudo-3D [15]N–[1]H-resolved NOESY correlations will arise. In all cases, cross-relaxation occurs during these MT processes, while water [1]Hs repolarize the targeted iminos resulting in sensitivity enhanced cross-peaks. Further enhancements are achieved through the Hadamard processing. "dec" refers to GARP4[19] or adiabatic[20] decoupling used during the encoding and the acquisition for labeled samples; water suppression was achieved using excitation sculpting[21] or WATERGATE-3139.[22–24] The water suppression block can be replaced with a selective spin-echo if detecting solely correlations among the imino protons.

While these calculations suggest that multiple selective inversions enable a full separation of NOEs via Hadamard encoding without cross-talk artifacts, this only holds in the limit of complete spin re-equilibration between scans. Should this not be the case, partial saturations driven by multiple looped inversions may also accumulate, and spread out to unselected (i.e., passive) protons. This will then lead to a situation as described above for Hadamard encoded continuous multiple-site saturations, and hence to cross-talk artifacts.

This point is clearly visible in Figure 3, which shows a series of SMT and HMT experiments carried out on the imino resonances of 5_SL5b+c –an RNA fragment taken from the SARS-CoV-2 viral genome. While artifact-free cross-relaxation traces arise from both SMT or from pulsed HMT encoding experiments carried without looping (Figure 3, grey and blue spectra), artifacts in the form of negative cross-peaks are evident in both the continuous saturation and looped inversion versions of the HMT acquisition (Figure 3, black and red traces). The reason for this is common and lies in the fact that, as highlighted by the red terms in Eq. (2), Hadamard-encoded saturation is not compatible with a clean Hadamard-decoded separation. Thus, when multiple inversions are applied on sites that do not exchange with the solvent fast enough, polarizations that were inverted may not be fully recovered by the start of the next loop. That's why the narrower resonances in this RNA (Figure 3, grey region), corresponding to sites that are in slower exchange with the water, lead to the strongest spurious cross-peaks. By contrast, broader RNA imino resonances corresponding to sites that are exchanging more rapidly with the solvent, lead to artifact-free reconstructions after the full Hadamard procedure (Figure 3b); these sites managed to replenish their magnetizations in-between every inversion pulse.

It follows that, as heretofore presented, neither saturation nor inversion procedures offer a foolproof way of exploiting Hadamard multiplexing in MT experiments within a group of cross-relaxing, exchanging sites. The present study proposes a solution to this problem, that exploits the enhancements arising from exchanges with the solvents, benefits from the multiplexing advantages of Hadamard encoding both for the intra-labile (e.g., imino-imino) and labile/non-labile (e.g., imino-amino/aromatic) NOE peak correlations, and does not suffer from the spurious artifacts just described regardless of whether solvent exchanges are fast or slow.
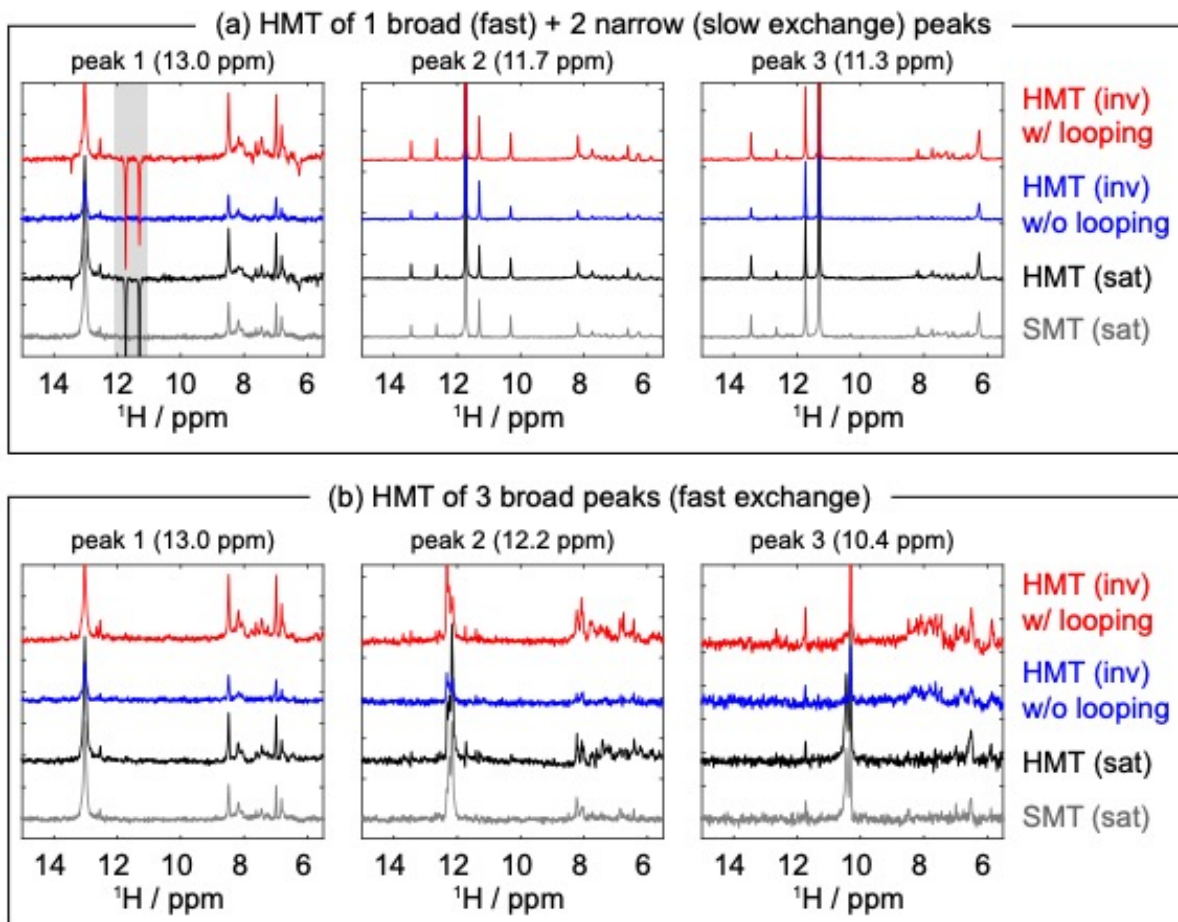
Figure 3. 1D slices extracted from SMT and HMT experiments targeting: (a) One fast (13.0 ppm) and two slow-exchanging (11.7 and 11.3 ppm) protons. (b) Three fast-exchanging protons. All experiments focused on the 5_SL5b+c RNA fragment of SARS-CoV-2, and were carried out at 1 GHz. SMT and regular HMT-saturation spectra (gray and black) were acquired using 800 ms saturation pulses ($\omega_1/2\pi$ = 8 Hz; see *Experimental Section*). HMT experiments without looping (blue) inverted the selected imino peaks with a *sinc* pulse (50 Hz bandwidth) followed by 175 ms mixing; in HMT with looping, polychromatic inversion pulses and a 125 ms mixing time were repeated 7 times. Note that artifacts do not appear in the looped pulsed HMT for rapidly exchanging (broad) peaks, but appear when targeting slowly exchanging (narrow) peaks. Notice as well that: (i) despite having equal number of scans the various experiments have remarkably different sensitivities: (ii) in agreement with the original Kupče & Freeman's original Hadamard-encoded NOESY proposition,[17] no artifacts are observed in inversion-based Hadamard without looping.

The Extended Hadamard Encoding Scheme

The arguments above explain why two distinct MT approaches were previously introduced to enhance sensitivity for cross-relaxation experiments on labile protons in biomolecules: a less sensitive but generalizable and artifact-free SMT scheme, was proposed for intra-set NOE correlations (as between RNA's imino protons); while a more sensitive but artifact-prone HMT scheme with multiply frequency-selective excitation (saturation or inversion) and Hadamard encoding, was proposed for inter-set NOE correlations (as between

RNA's imino and amino protons). As derived above, however, artifacts may occur whenever multiple protons within a cross-relaxing proton network are perturbed simultaneously, leading to inseparable non-linear responses when using conventional Hadamard encoding to tackle, for instance, imino-imino correlations. To fully disentangle such complex responses, we here introduce an "extended Hadamard" encoding scheme that allows recording artifact-free cross-relaxation experiments on both like and unlike proton groups, with the combined sensitivity enhancement from multiplexing (Hadamard editing) and continuous repolarization via water exchange.

Even if other biomolecular scenarios are conceivable, we shall consider for concreteness the imino→imino and imino→amino correlations encountered in the RNA-based examples here presented. We thus consider a system with n_I imino protons of initial polarization I, that can have cross peaks with amino protons of initial polarization A. If the ith imino proton is saturated the polarization A of an amino proton 'a' that cross-relaxes with it changes as $A \rightarrow A - \Delta A_i$, and if A cross-relaxes with two or more imino protons that are simultaneously saturated we assume that its change in polarization is linear; i.e., if one saturates i and j iminos cross-relaxing with A, then $A \rightarrow A - \Delta A_i - \Delta A_j$. To disentangle the correlations of the n_I iminos a series of n_S ($n_S \geq n_I$) scans will be recorded, where each involves the saturation of some, none, or all imino protons. If this saturation proceeds according to Hadamard encoding strategy as described in the Introduction, the experiment will be defined by an $n_S \times n_I$ matrix $C = \{c_{lm}\}_{l=1:n_S, m=1:n_I}$ where $c_{lm} = -1$ if in the lth scan the mth proton is saturated, and $c_{lm} = +1$ otherwise. The signal of the amino proton 'a' observed in scan l will be

$$S_l^a = A + \sum_{i=1}^{n_I} (c_{li} - 1) \frac{\Delta A_i}{2} \tag{5}$$

The ΔA_i contributions arising from the iminos are then disentangled according to the Hadamard strategy in the Introduction, whereby the desired cross peak with amino site 'a' associated to a particular imino proton i, C_i^a, is obtained as

$$C_i^a = \sum_{l=1}^{n_S} c_{li} S_l^a = \sum_{l=1}^{n_S} c_{li} \left(A + \sum_{m=1}^{n_I} (c_{lm} - 1) \frac{\Delta A_m}{2} \right) \tag{6a}$$

$$= \sum_{l=1}^{n_S} c_{li} A + \sum_{l=1}^{n_S} \sum_{m=1}^{n_I} c_{li}(c_{lm} - 1) \frac{\Delta A_m}{2} \tag{6b}$$

The fact that the numbers of +1 and -1 in each column of a standard Hadamard matrix are equal, implies that $\sum_{l=1}^{n_s} c_{li} = 0$ for any column i; i.e., that no relaxed A signal (first term on Eq. (6b)) will contribute to the final spectrum. The orthogonality between any two columns of a Hadamard matrix also implies that $\sum_{l=1}^{n_s} c_{li}c_{lm} = 0$ for $m \neq i$, meaning that out of all the terms in the double summation of Eq. (6b) the sole surviving products are those involving $m = i$. As there are n_S such terms it follows that

$$C_i^a = n_s \frac{\Delta A_i}{2} \tag{7}$$

which is as expected from the arguments in the Introduction: only the contribution of the ith imino proton that we assumed cross-relaxing with A shows up, amplified by half the number of scans as a result from the Hadamard multiplexing.

Consider now a similar scenario but aimed at establishing the imino-imino cross peaks. To do so we assume a linearity in the site's cross-talks: i.e., we assume that if the qth imino proton is saturated, the polarization of a pth cross-relaxing imino peak I_p will change as $I_p \rightarrow I_p - \Delta I_{pq}$; and that if two (or more) iminos q and r are saturated and cross-relax with proton p, then the change in the latter will be $I_p \rightarrow I_p - \Delta I_{pq} - \Delta I_{pr}$. The signal corresponding to the pth imino proton obtained in scan l can then be written as

$$S_l^p = I_p + (c_{lp} - 1)\frac{I_p}{2} + \sum_{m=1}^{n_I} (c_{lp} + 1)(c_{lm} - 1)\frac{\Delta I_{pm}}{4} \tag{8}$$

If applying on these signals the same $C_q^p = \sum_l c_{lq} S_l^p$ Hadamard decoding strategy as above, the cross-peak at imino site p associated to imino site q becomes

$$C_q^p = \sum_{l=1}^{n_S} c_{lq} \left\{ I_p + (c_{lp} - 1)\frac{I_p}{2} + \sum_{m=1}^{n_I} (c_{lp} + 1)(c_{lm} - 1)\frac{\Delta I_{pm}}{4} \right\} \tag{9}$$

As before, the $\sum_{l=1}^{n_s} c_{lq} = 0$ and $\sum_{l=1}^{n_s} c_{lq}c_{lp} = 0, p \neq q$ conditions imply that all contributions of the initial polarization I_p will cancel out, as desired. The inter-imino cross-peaks, however, now involve a new product between *three* encoding coefficients

$$\sum_{l=1}^{n_S} c_{lq}(c_{lp} + 1)(c_{lm} - 1) = 0, \qquad q \neq p \neq m. \tag{10}$$

Linear and quadratic combinations of these coefficients will cancel out upon summation for every combination of different spin pairs, as desired. To remove all but the pairwise cross-relaxation contributions, one now also demand the additional request

$$\sum_{l=1}^{n_S} c_{lq} c_{lp} c_{lm} = 0 , \qquad q \neq p \neq m, \tag{11}$$

a condition that is new, and did not arise when considering imino→amino cross-peaks.

Eq. (11) poses a demand that is not fulfilled by Hadamard matrices in their standard form. We therefore sought out a matrix for which this third condition is satisfied for a given n_I number of imino sites, while still retaining Hadamard original matrix orthogonality condition. Suitable solutions fulfilling all these three demands are provided by what we denote as *extended* Hadamard matrices E, which we built from smaller Hadamard encodings by an extension of the original Hadamard matrices, involving a negation of all experiments involved. Thus, for example for $n_I \leq 4$ sites, an 8×4 extended Hadamard matrix E which satisfies all expectations involved by both imino→amino and imino→imino HMT experiments, arises from

$$E_4 = \begin{bmatrix} H_4 \\ -H_4 \end{bmatrix} = \begin{bmatrix} 1 & 1 & 1 & 1 \\ 1 & -1 & 1 & -1 \\ 1 & 1 & -1 & -1 \\ 1 & -1 & -1 & 1 \\ -1 & -1 & -1 & -1 \\ -1 & 1 & -1 & 1 \\ -1 & -1 & 1 & 1 \\ -1 & 1 & 1 & -1 \end{bmatrix} \tag{12}$$

where H_4

$$H_4 = \begin{bmatrix} 1 & 1 & 1 & 1 \\ 1 & -1 & 1 & -1 \\ 1 & 1 & -1 & -1 \\ 1 & -1 & -1 & 1 \end{bmatrix} \tag{13}$$

is the standard 4×4 Hadamard matrix. The first row of E_4 corresponds to no saturation, its rows 2-4 and 6-8 contain all possible double saturations, and row 5 corresponds – paradoxically– to the saturation of all targeted protons. The form of E in Eq. (12) suggests how to extend this kind of encoding to more numerous sites. Thus, for instance, if addressing $4 \leq n_I \leq 8$ sites requires from conventional Hadamard to employ an 8×8 matrix

$$H_8 = \begin{bmatrix} H_4 & H_4 \\ -H_4 & H_4 \end{bmatrix}, \tag{14}$$

then performing an extended Hadamard transform will require a 16×8 matrix

$$E_8 = \begin{bmatrix} H_8 \\ -H_8 \end{bmatrix} = \begin{bmatrix} H_4 & H_4 \\ H_4 & -H_4 \\ -H_4 & -H_4 \\ -H_4 & H_4 \end{bmatrix} \tag{15}$$

where if $n_I < 8$, the encoding strategy calls for using the first n_I rows of E_8. When utilizing any of these extended forms, one can deduce the change in polarization of an amino proton a due to cross-relaxation by an imino proton i, by implementing the sums in Eqs. (5-6) along all of E columns:

$$C_i^a = \frac{n_S}{2}\Delta A_i \quad ; \quad (16)$$

this is just as in the original Hadamard processing. Similarly, as the conditions $\sum_l c_{lq}c_{lp}c_{lm} = 0$, $q \neq p \neq m$ are now also satisfied, the reconstructed cross-peak intensity expected at imino site p due to cross-relaxation with an imino proton q, will be

$$C_q^p = \frac{n_S}{4}\Delta I_{pq} \quad ; \quad (17)$$

this is only half as efficient as the imino→amino encoding (Eq. (16)), but will now arise without undesirable contaminations. It is clear to envision how a similar strategy, may allow extensions of this approach to the encoding of $n_I \geq 9$ sites.

Notice that by contrast to conventional Hadamard encoding, this extended Hadamard mode calls for recording at least twice the number of experiments (n_S) as sites are present in the correlations. If –as is almost invariably the case– the NOE correlations being sought are a sensitivity-limiting factor and more than the minimum $n_S = n_I$ number of scans needs to be collected anyhow, then, in practice, this will not be a penalty. This, provided that the additional number of scans demanded by the extended HMT (eHMT) procedure, still enjoys Hadamard multiplexing advantages. For the amino→imino correlations this will clearly be the case, as the cross-peak strength after n_S scans in Eqs. (7) (HMT) and (16) (eHMT), are the same. As HMT did not work for imino→imino correlations, the point of comparison for the latter is the SMT case –which is an on/off magnetization transfer difference experiment carried out on each of the $1 \leq i \leq n_I$ imino protons. Since the number of scans in the standard SMT experiment is $2n_I$ (akin to STD, SMT is a difference experiments, and hence requires at least two scans per addressed site), while extended HMT (which, unlike SMT, does not require taking differences against a reference scan) requires $n_S > n_I$ scans, it is easiest to arrive at a signal-to-noise per scan comparison, by assuming that both experiments are carried out for the same total number of scans $2n_I n_S$ –meaning that in the SMT case, n_S scans were averaged for each site. Denoting as N_1 the noise in one scan, the SNR of a cross peak at imino site p due to imino site q in the SMT experiment will then be

$$SNR_{SMT} \propto \sqrt{n_S} \cdot \frac{\Delta I_{pq}}{\sqrt{2} \cdot N_1} \quad (18)$$

while its eHMT counterpart will be

$$SNR_{eHMT} \propto \frac{C_q^p}{\sqrt{n_S} \cdot N_1} \sqrt{2n_I} = \frac{\sqrt{n_S}}{4 \cdot N_1} \sqrt{2n_I} \cdot \Delta I_{pq} \quad (19)$$

It follows from here that eHMT imino→imino enhancement in *SNR* per unit time (scan), ϵ_I, will be

$$\epsilon_I = \frac{SNR_{eHMT}}{SNR_{SMT}} = \frac{\sqrt{n_I}}{2} \quad (20)$$

It is thus seen that there will be an SNR advantage, $\epsilon_I > 1$, for $n_I > 4$.

Assessing Homonuclear Magnetization Transfers in RNA fragments: SMT *vs* HMT *vs* eHMT *vs* NOESY

SMT, HMT, eHMT and conventional 2D NOESY experiments were implemented on the 5_SL5b+c RNA fragment derived from the SARS-CoV-2, seeking NOE correlations between the imino protons and other nearby protons at 1 GHz and 283K. This fragment derives from the 5'-terminal untranslated region (5'-UTR) of the SARS-CoV-2 RNA genome, known to be highly structured and conserved among Betacoronaviruses.[25] The regulatory function of 5'-UTR has been linked to the maintenance of viral replication, balanced transcription of subgenomic mRNAs and translation of viral proteins, and it is being evaluated as potential targets of low molecular weight drugs.[26] As ^{1}H assignments for this RNA fragment have been reported,[27] experiments were carried out mainly to examine the presence of artifacts and relative sensitivities. As already demonstrated in Ref [14] the most basic of these experiments, SMT, will significantly enhance cross-relaxation peaks when compared to its conventional counterpart; under the assayed conditions (grey vs black traces in Figure 4), ca. 4- and 6-fold SNR enhancements per unit time (SNRT) were observed for imino-imino and imino-amino proton correlations, respectively.[†] Regular HMT shows even larger SNRT enhancements for imino-amino cross-peaks, yet clear artifacts are also visible, particularly for the imino-imino cross-peaks. eHMT can solve this problem, providing clean, artifact-free spectra with genuine correlations (red spectra in Figure 4). As this RNA fragment contains a total of 12 imino peaks, two sets of E_8 (Eq. [15]) or three sets of E_4 (Eq. [12]) eHMT matrices could be used for these acquisitions, encoding 6 or 4 peaks, respectively. For the latter case, the required number of scans (n_s) becomes 3 x 8 = 24; i.e., it

---

[†] We rely in this study on SNR/unit_time rather than on the more customary SNR/sqrt(unit_time) criterion used in Fourier-transform NMR, due to the hybrid Fourier/non-Fourier nature of the various experiments here compared. In any case, Table 1 provides all the information needed to compute either metrics.

requires more scans than a regular HMT acquisition for which $n_s = 16$. In accordance to the derivations above eHMT shows then a lower sensitivity per unit time (or per scan) than regular HMT (Table 1): whereas the average SNRT of imino-amino correlations is 22.3 for regular HMT, it is 14.7 for eHMT case. Also as predicted [Eq. (19)] eHMT achieves higher enhancements as the number of encoded peaks (n_I) in the matrix grows: For the E_8 matrix encoding up to 8 peaks, ~1.4x larger SNRT was observed on the cross-peaks, than when encoding with three E_4s.

Higher SNRT enhancements are achievable for imino-imino correlations if the WATERGATE 3139 block in Figure 2, is replaced with a selective spin-echo optimized to excite/refocus signals solely the imino spectral region. Although correlations on the amino
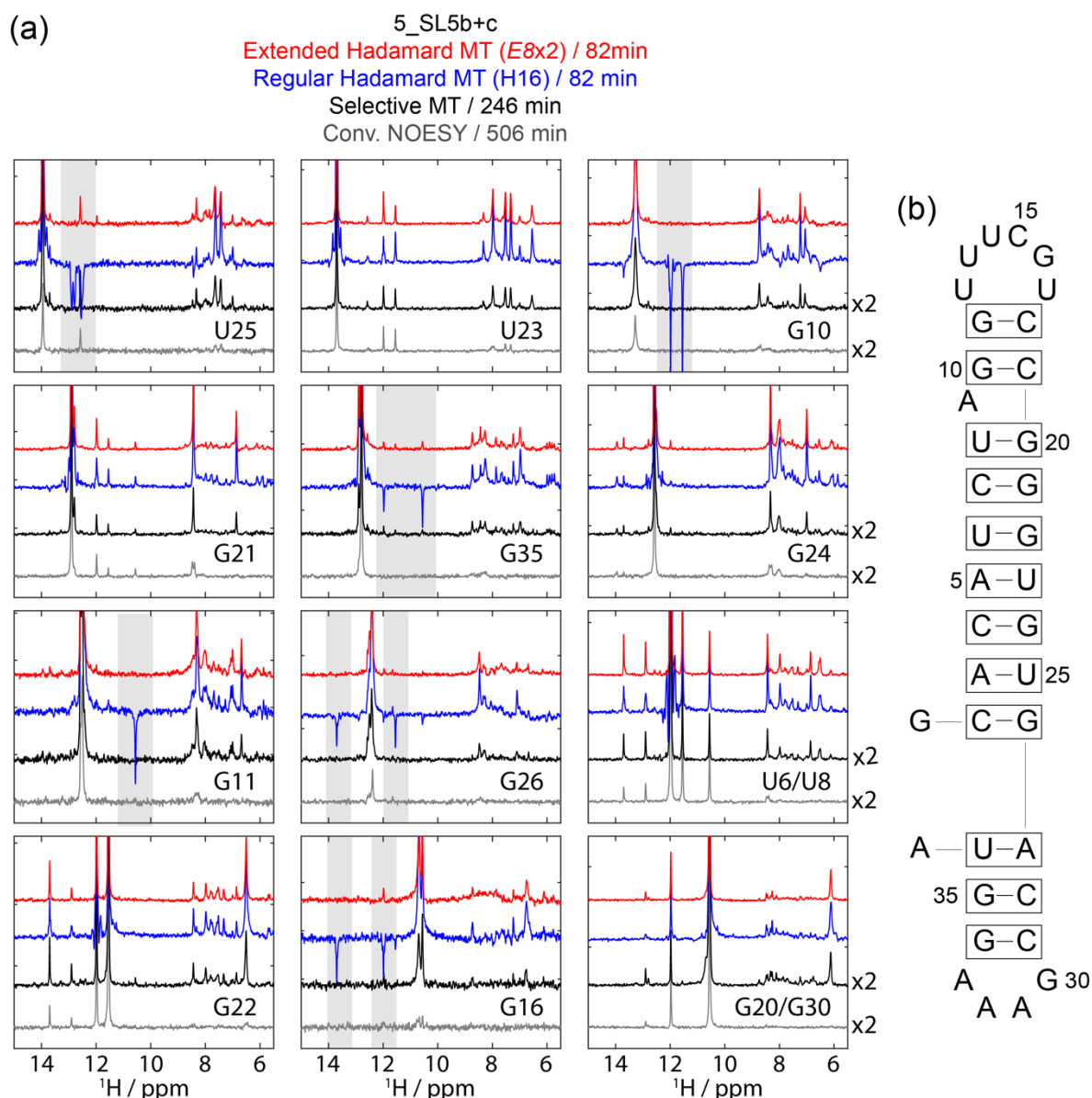

Figure 4. (a) Comparison between cross-relaxation spectra extracted for the indicated imino protons in the SARS-CoV-2-derived 5_SL5b+c RNA fragment in (b), measured using regular Hadamard MT

(blue), SMT (black), extended HMT (red), and conventional NOESY (gray). All MT spectra were acquired using an 800 ms saturation time, while the conventional NOESY was recorded with a 150 ms mixing time. All experiments were performed at 1 GHz NMR at 283 K. The averaged SNR and SNRT for each trace are summarized in Table 1.

protons' spectral region are then lost, a shorter interscan delay can be used, further increasing sensitivity during the same experimental time. Figure S1 (Supporting Information) compares eHMT imino-imino NOE correlation spectra measured with selective spin-echo (SE) and WATERGATE (WG) pulse sequences. Note that the SE-based experiment shows ≈2x higher SNR, though requiring only half of the experimental time than WG-based experiments. Averaged SNR and SNRT enhancements for these experiments are also quantified in Table 1. These SE eHMT experiments could be particularly useful for revealing sequential connectivity in DNAs and RNAs from imino-imino NOE correlations, which is a first step in determining secondary structures.
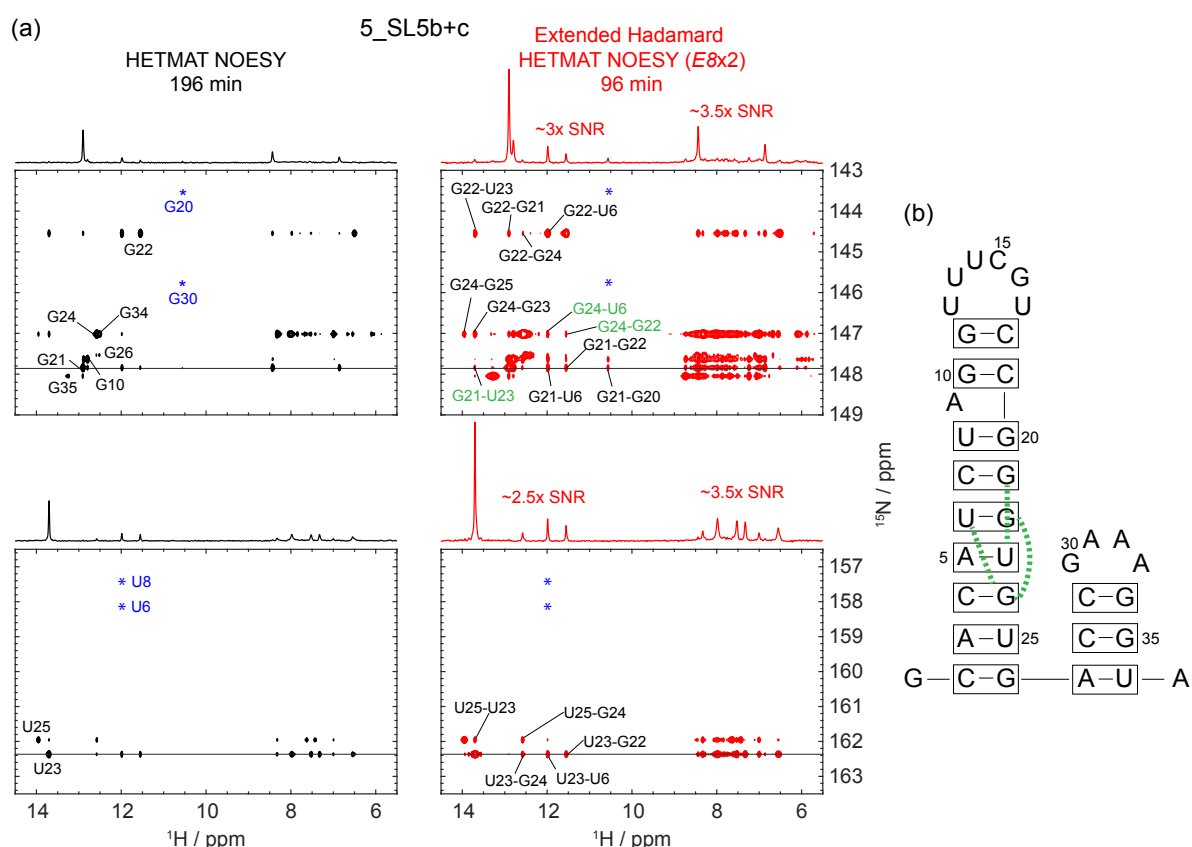

Figure 5. (a) Comparison between HETMAT (left, black) and extended Hadamard HETMAT NOESY (right, red) showing imino-imino and imino-amino proton correlations for the SARS-CoV-2-derived 5_SL5b+c RNA fragment in (b) measured at 1 GHz and 283 K. To build up a 2D spectrum, each 1D spectra were placed into ^{15}N-^{1}H plane according to the ^{15}N chemical shifts of selected ^{15}N-^{1}H spin pair. Assignments reported for diagonal peaks are annotated in the left panel, and cross-peaks are labeled in the right panel. Among the cross-peaks, newly observed ones are labeled in green. Blue asterisks indicate the peaks excluded in the Hadamard experiments due to the overlapping along with the ^{1}H chemical shift. In HETMAT experiment, RF CP field $\omega_1/2\pi$ of 75 Hz with 20 loops, τ_{NOE} = 30

ms and 50 Hz with 7 loops, τ_{NOE}= 125 ms were used for the broader and narrow peaks, respectively. In Hadamard experiment, RF CP field $\omega_1/2\pi$ = 20 Hz with 7 loops and a τ_{NOE}= 125 ms was used for all peaks. 1D slices at selected ^{15}N chemical shift are shown in each panel. The averaged enhancements of SNR and SNRT are summarized in Table 1. Comparisons between these spectra and spectra from 2D HMQC NOESY and regular Hadamard HETMAT NOESY, are shown in Supporting Information (Figure S6). (b) Secondary structure of 5_SL5b+c; dashed lines denote the new correlations observed in extended Hadamard HETMAT between base pairs.

The eHMT scheme can also be used as starting point for encoding more complex experiments. To illustrate this, the extended Hadamard scheme was adapted to HETMAT NMR,[13] a pseudo-3D acquisition that also relies on magnetization transfers. Unlike SMT/HMT experiments, imino protons of interest are here selected for saturation in a 2D $^1H/^{15}N$ plane, using a frequency-specific 2D cross-polarization (CP) saturation module (Figure 2b) –leading essentially to a 3D version of HSQC-NOESY. When extending this site-specific saturation scheme to a Hadamard version where multiple peaks are perturbed simultaneously, an additional source of artifact (besides that mentioned above) can arise, stemming from unintended cross-talks between the sites. During the course of these tests we found that the site selectivity afforded by a low-power CP executed with $\omega_1/2\pi$ = 50 Hz fields –which was sufficient in the site-by-site HETMAT experiments we described at 1 GHz[13]– became insufficient to provide clean spectra after Hadamard reconstruction (Figure S2). Therefore, all extended Hadamard HETMAT (eHETMAT) experiments were performed with CP $\omega_1/2\pi$ = 20 Hz; although this narrower CP would be associated with a sensitivity loss, it might be compensated by the SNR enhancements achieved from the Hadamard scheme.

In the original HETMAT, every second scan was a reference scan where CP was applied at a far off-resonance ^{15}N chemical shift. Only the targeted peak was inverted by subtracting on- and off-resonance scans, while the effects arising from the peaks overlapping along either ^1H or ^{15}N chemical shift were canceled out. By contrast in the Hadamard version of the experiment subtraction occurs between spectra encoded by the Hadamard matrix – without the benefits of an independent, reference scan. If the various peaks being encoded have different ^1H chemical shifts, genuine cross-peaks are easily identified by comparing the resulting spectra, as illustrated in Figure S3. However, if two peaks to be correlated happen to be overlapping in the ^1H dimension, it is not simple to distinguish among their cross-peaks in the absence of a reference scan. As HETMAT-based tests of the extended Hadamard ideas we therefore decided to exclude overlapping ^1H peaks out of the current discussion, and grouped peaks in the different Hadamard experiments with as little overlap as possible. Supporting Figures S4 and S5 show how these peaks were grouped for the 5_SL5b+c and the

larger 5_SL8 RNA fragments of SARS-CoV-2, by marking them with the same color in their 2D HSQC spectra. A full spectrum can then be reconstructed simply by adding the Hadamard sub-spectra.

The performance of eHETMAT NOESY experiments is illustrated in Figures 5 and 6, when targeting 5_SL5b+c and 5_SL8 RNA fragments, respectively. For 5_SL5b+c, a total of 9 peaks were encoded with either three sets of extended Hadamard matrices E_4 (Eq. [12]), or two sets of E_8 matrices (Eq. [15]). Using reported assignments,[27] all the diagonal and cross-peaks for 5_SL5b+c could be identified and no artifacts were noticed (Figure 5). These data emphasizes the sensitivity enhancement that extended Hadamard HETMAT NOESY provides over its original proposition; Table 1 lists the average SNR and SNRT performances for both experiments, showing that the addition of Hadamard encoding can enhance SNR by 2-3.5x, in measurements that have ca. half the acquisition times. This is clearly visible in the 2D contour plot, and in the comparisons among 1D slices obtain with and without the extended Hadamard encoding shown in Figure 5a and in Supporting Figure S6. These reveal that several imino-imino correlations that are detected in eHETMAT, are invisible in both conventional NOESY/HSQC and in non-Hadamard HETMAT experiments (green labels in Figure 5a).

For the larger 5_SL8 RNA fragment, a total of 12 peaks were selected and encoded into two sets of extended Hadamard HETMAT E_8 matrices. As shown in Figure 6, all diagonal and cross-peaks were identified by the eHETMAT NOESY experiment without noticeable artifacts, while showcasing superior sensitivity and shorter experimental times than non-Hadamard counterparts. Several additional correlations for peaks that are still lacking an unambiguous assignment (labeled as GA, GB, GC, GD, UA, UB, and UC in Figure 6), could also be detected. However, the spectral denseness arising in this relatively large RNA fragment, compromises the resolution of even this pseudo-3D HSQC/NOESY-type acquisition. Further evaluation of structure and dynamics for 5_SL8 will require the even higher dimensional experiments, which we are developing while still using the benefits from the presented eHETMAT approach.

Discussion and Conclusions

An extended Hadamard scheme was introduced to obtain sensitivity-enhanced NOE correlations between labile sites and between labile and non-labile sites, and demonstrated by targeting the imino protons in SARS-CoV-2 RNA fragments. The need to develop these schemes arose from artifacts created by the original HMT, when trying to obtain clean

correlations between perturbated labile sites. The extended Hadamard method presented here provides a solution to this problem, allowing one to enjoy both Hadamard multiplexing advantage as well as the CEST-like cross-peak enhancements arising from solvent exchanges. This was achieved by extending the regular Hadamard matrix to fulfill a new condition, $\sum_l c_{lq} c_{lp} c_{lm} = 0$, $q \neq p \neq m$ that is not required for detecting other types of Hadamard-encoded correlations. Though requiring at least twice as many experiments as the regular Hadamard encoding, this method also provided substantial SNR/unit_time gains relative to the conventional counterparts. The extended Hadamard scheme was compatible with ^{1}H-^{1}H and ^{1}H-^{15}N-^{1}H HETMAT experiments, leading to pseudo-2D NOESY and pseudo-3D HSQC-NOESY experiments. The resulting sensitivity gains revealed new imino-imino
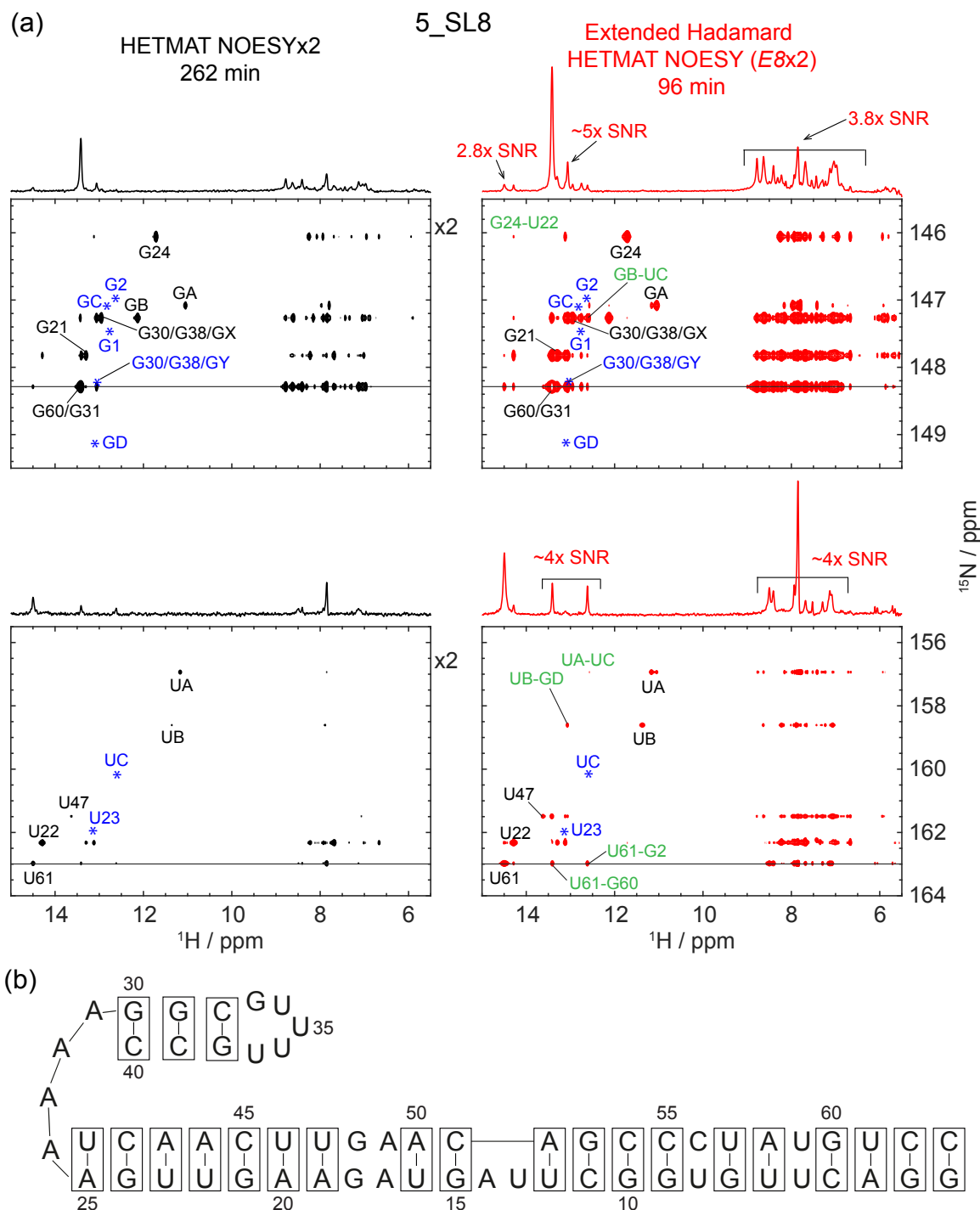
Figure 6. Idem as in Figure 5, but for the larger 5_SL8 fragment shown in (b). Assignments reported for diagonal peaks are annotated in both panels in black and blue, with the latter excluded from the extended Hadamard HETMAT experiments due to overlap along the ^{1}H dimension. Unassigned peaks are labeled GA, GB, GC, GD, UA, UB, and UC. The right-hand panels show in green cross-peaks observed by eHETMAT but not in the non-Hadamard experiment. For the HETMAT, RF CP fields $\omega_1/2\pi$ = 75 Hz with 17 loops and a τ_{NOE} = 50 ms were used for addressing the broader peaks, while 50 Hz with 10 loops with τ_{NOE} = 80 ms mixing was used for the rest of the peaks. In the Hadamard experiments, RF CP fields $\omega_1/2\pi$ = 20 Hz with 10 loops and a τ_{NOE} = 80 ms were used. 1D slices at selected ^{15}N chemical shift are shown on top. Note that intensities in 2D contour plot and 1D slices of HETMAT NOESY (black) are multiplied by a factor of 2. The averaged enhancements of SNR and SNRT are summarized in the Table 1. Comparisons between these spectra and spectra from 2D HMQC NOESY and regular Hadamard HETMAT are shown in Supporting Information Figure S7.

correlations that were not visible in conventional or in SMT-based NOESY experiments. Not only imino-imino correlations in RNAs but also correlations between amide protons on proteins could be examined using this method, which would be useful to elucidate their structures. While correlations between hydroxyl protons such as in sugar moieties would not be detectable due to fast exchanging with solvent protons, cross-peaks arising from these protons to other types of protons (CH or NH) would be detectable, expecting the similar SNR enhancements as illustrated here. The extended Hadamard concepts introduced here could also be included in higher dimensional experiments, providing additional resolution as pseudo-3D or pseudo-4D experiments involving OH or NH protons. This option is currently being explored.

Despite the advantages stated above, the extended Hadamard method has drawbacks and limitations. Unlike SMT or HETMAT experiments where saturation/inversion fields, mixing time, and the number of loops to be chosen can be tailored peak-by-peak, Hadamard multiplexing as we have implemented here uses single, common parameters for addressing all selected sites. This may result in a loss of efficiency for transferring polarization through NOE, as equal parameters are applied for both narrow and broad peaks. This problem could simply be solved by separating the eHMT encoding into blocks, addressing peaks based on their common rates of solvent exchange (i.e., on their linewidths). Two such sets of different parameters should be sufficient to detect cross-peaks with full sensitivity. Otherwise, fine-tuning of the irradiation scheme to have multiple frequencies with distinct strengths, could also be incorporated into the saturation experiment. For the inversion cases -whether dealing with HMT- or HETMAT-based inversions– the application of this scheme might be less useful as it would have to involve tailoring the number of loops for each site, rather than the strength of the irradiation. Still, some of these features are currently being explored.

As other frequency-selective experiments also eHMT, like SMT and HETMAT, benefits from performance at the highest possible magnetic fields –where a maximum site resolution is available to separate peaks and to prevent cross-talks, and were larger fields can lead to better inversions/saturations. For instance, a 20 Hz Hartmann-Hahn match shows sufficient selectivity to avoid cross-talks in HETMAT experiments at 1 GHz, but not at 500 MHz (Figure S8). Moreover, dealing with large number of peaks decreases the relative advantage of all these frequency-encoded experiments vs their time-domain counterparts. Solutions to these remaining complications are being sought.

Experimental Section

Sample preparation. ^{15}N-labeled 5_SL5b+c and 5_SL8 RNA samples were produced by T7 polymerase-based *in-vitro* transcription, as described in Ref [27]. RNA purity was verified by denaturing PAA gel electrophoresis and homogenous folding was monitored by native PAA gel electrophoresis. The final concentration of the 5_SL5b+c and 5_SL8 samples in the NMR tubes were 0.7 and 0.8 mM, respectively.

NMR experiments. NMR experiments were run on a 1 GHz, 23.5 T Bruker Avance Neo spectrometer equipped with a TCI cryoprobe. All pseudo-2D SMT and pseudo-3D HETMAT NOESY experiments were performed following previously described procedures.[13,14] In SMT, the duration of the saturation pulse was set to 800 ms, with 8 Hz and 30 Hz $\omega_1/2\pi$ fields to saturate narrow and broader imino resonances, respectively. For the HMT experiments, all peaks were saturated with pulses of the same duration but 8 Hz nutation fields. The nutation frequencies and CP duration of the HETMAT experiments were chosen as 50 Hz / 14.5 ms or 75 Hz / 10.4 ms, depending on the broadness of peaks; 20 Hz / 46 ms were used in the eHETMAT experiments. The mixing time and number of loops were optimized depending on the sample, to achieve a maximum NOE: NOESY mixing times ranging from 150-200 ms were utilized in the conventional experiments for both homonuclear 2D NOESY and 2D HMQC-NOESY experiments. Spectra were acquired with 512 scans for SMT and HETMAT; 64 or 128 scans for the Hadamard-based experiments. Each spectrum was apodized with a QSINE window function and Fourier transformed using Topspin software (Bruker Biospin). Importing the peak list into the Hadamard experiment was performed using au-programs "had_pl" and "had_plx" for HMT and Hadamard HETMAT experiments, respectively. All pulses were generating using WaveMaker via the "wvm -a" that is based on the regular Hadamard matrix. For using extended Hadamard matrice, "wvm_x" was used, that generates pulses based on the user-defined Hadamard matrix, saved in a "wvm.had" file by the experiment. Spectra were processed using custom-written au-program "proc_had" for HMT and "proc_hadx" for Hadamard HETMAT directly in TopSpin 4.0.9. SMT and HETMAT spectra were processed in similar ways, after zero-filling to 512 F_1 points. Supporting Table S1 summarizes the main parameters used in all types of experiments shown in this study. Additional experimental details, including experimental set-up and pulse sequences implementation, can be downloaded from https://www.weizmann.ac.il/chembiophys/Frydman_group/software.

Table 1. SNR and SNR/unit_time (SNRT) enhancements extracted upon comparing HMT and conventional cross-relaxation experiments.

Sample	Total # peaks	Type of experiment	Total # scan	Acquisition time	Avg SNR enh.[*][§] (imino/amino)	Avg SNRT enh.[*][§] (imino/amino)
WG-based NOESY experiment						
5_SL5b+c	12	eHMT ($E_8 \times 2$)	2048 (16 × 2 × 64)	82 min	3.7 / 9.5	8.5 / 23.7
		eHMT ($E_4 \times 3$)	3072 (8 × 3 × 128)	124 min	3.2 / 7.3	6.4 / 14.7
		Regular HMT (H16)	2048 (16 × 128)	82 min	- / 9.0[#]	- / 22.3[#]
		SMT	6144 (12 × 2 × 256)	246 min	2.9 / 4.3	4.2 / 6.1
		Conv. NOESY	32	506 min	-	-
Selective SE-based NOESY experiment (imino only)						
5_SL5b+c	12	eHMT ($E_8 \times 2$)	2048 (16 × 2 × 64)	41 min	2.6 / -	7.2 / -
		eHMT ($E_4 \times 3$)	3072 (8 × 3 × 128)	62 min	3.1 / -	7.0 / -
		SMT	6144 (12 × 2 × 256)	124 min	1.6 / -	2.5 / -
		Sofast NOESY	128	309 min	-	-
HETMAT NOESY experiment						
5_SL5b+c	9	eHETMAT ($E_8 \times 2$)	2048 (16 × 2 × 64)	96 min	7.2 / 4.3	13.3 / 7.9
		eHETMAT ($E_4 \times 3$)	3072 (8 × 3 × 128)	144 min	7.8 / 4.7	11.7 / 7.0
		Regular Hadamard HETMAT (H16)	2048 (16 × 128)	96 min	- / 4.1[#]	- / 7.5[#]
		HETMAT	4608 (9 × 2 × 256)	196 min	4.8 / 1.5	6.1 / 2.0
		Conv. HMQC-NOESY	28	323 min	-	-
5_SL8	12	eHETMAT ($E_8 \times 2$)	2048 (16 × 2 × 64)	96 min	8.4 / 13.2	14.3 / 22.4
		Regular Hadamard HETMAT (H16)	2048 (16 × 128)	95 min	- / 13.8[#]	- / 23.6[#]
		HETMAT	6144 (12 × 2 × 256)	262 min	7.8 / 2.6	8.0 / 2.7
		Conv. HMQC-NOESY	24	277 min	-	-

[*] $SNR\ enh = \frac{SNR_{Hadamard\ or\ SMT}}{SNR_{Conv.\ NOESY}}$, $SNRT\ enh = \frac{SNR_{Hadamard\ or\ SMT}/\sqrt{Acquisition\ time}}{SNR_{Conv.NOESY}/\sqrt{Acquisition\ time}}$ and its averages are calculated as $\frac{\sum SNR(T)enh.}{N}$ for N peaks.

[§] Cross-peak not detected in SMT or HETMAT; a minimum 10-fold enhancement is assumed and then averaged.

[#] Due to artifacts on regular Hadamard experiment, SNR and SNRT enhancements were calculated only for amino peaks.

References

[1] J. Jeener, B. H. Meier, P. Bachmann, R. R. Ernst, *J. Chem. Phys.* **1979**, *71*, 4546–4553.

[2] W. P. Aue, E. Bartholdi, R. R. Ernst, *J. Chem. Phys.* **2008**, *64*, 2229–2246.

[3] A. W. Overhauser, *Phys. Rev.* **1953**, *92*, 411–415.

[4] K. Wüthrich, *NMR of Proteins and Nucleic Acids*, Wiley, New York, **1986**.

[5] S. Macura, W. M. Westler, J. L. Markley, in *Methods Enzymol.*, Academic Press, **1994**, pp. 106–144.

[6] J. Cavanagh, Ed. , *Protein NMR Spectroscopy: Principles and Practice*, Elsevier, Acad. Press, Amsterdam, **2007**.

[7] L. Braunschweiler, R. R. Ernst, *J. Magn. Reson. 1969* **1983**, *53*, 521–528.

[8] A. Bax, D. G. Davis, *J. Magn. Reson. 1969* **1985**, *65*, 355–360.

[9] A. G. Palmer, J. Cavanagh, P. E. Wright, M. Rance, *J. Magn. Reson. 1969* **1991**, *93*, 151–170.

[10] A. Bax, R. H. Griffey, B. L. Hawkins, *J. Magn. Reson. 1969* **1983**, *55*, 301–315.

[11] M. Novakovic, S. F. Cousin, M. J. Jaroszewicz, R. Rosenzweig, L. Frydman, *J. Magn. Reson.* **2018**, *294*, 169–180.

[12] M. Novakovic, Ē. Kupče, A. Oxenfarth, M. D. Battistel, D. I. Freedberg, H. Schwalbe, L. Frydman, *Nat. Commun.* **2020**, *11*, 5317.

[13] J. Kim, M. Novakovic, S. Jayanthi, A. Lupulescu, E. Kupce, J. T. Grün, K. Mertinkus, A. Oxenfarth, C. Richter, R. Schnieders, J. Wirmer-Bartoschek, H. Schwalbe, L. Frydman, *J. Am. Chem. Soc.* **2021**, *143*, 4942–4948.

[14] M. Novakovic, Ē. Kupče, T. Scherf, A. Oxenfarth, R. Schnieders, J. T. Grün, J. Wirmer-Bartoschek, C. Richter, H. Schwalbe, L. Frydman, *Angew. Chem. Int. Ed.* **2021**, *60*, 11884–11891.

[15] E. I. Hyde, B. Birdsall, G. C. K. Roberts, J. Feeney, A. S. V. Burgen, *Biochemistry* **1980**, *19*, 3738–3746.

[16] E. Kupče, T. Nishida, R. Freeman, *Prog. Nucl. Magn. Reson. Spectrosc.* **2003**, *42*, 95–122.

[17] Ē. Kupče, R. Freeman, *J. Magn. Reson.* **2003**, *162*, 300–310.

[18] Ē. Kupče, R. Freeman, *J. Magn. Reson.* **2003**, *162*, 158–165.

[19] Z. Zhou, R. Kümmerle, X. Qiu, D. Redwine, R. Cong, A. Taha, D. Baugh, B. Winniford, *J. Magn. Reson.* **2007**, *187*, 225–233.

[20] R. Fu, G. Bodenhausen, *J. Magn. Reson. A* **1996**, *119*, 129–133.

[21] T. L. Hwang, A. J. Shaka, *J. Magn. Reson. A* **1995**, *112*, 275–279.

[22] V. Sklenar, M. Piotto, R. Leppik, V. Saudek, *J. Magn. Reson. A* **1993**, *102*, 241–245.

[23] M. Piotto, V. Saudek, V. Sklenář, *J. Biomol. NMR* **1992**, *2*, 661–665.

[24] G. Lippens, C. Dhalluin, J. M. Wieruszeski, *J. Biomol. NMR* **1995**, *5*, 327–331.

[25] D. Yang, J. L. Leibowitz, *Virus Res.* **2015**, 206, 120–133.

[26] S. Sreeramulu, C. Richter, H. Berg H, et al, *Angew Chemie Int. Ed.* **2021**, in press. anie.202103693

[27] A. Wacker, J. E. Weigand, S. R. Akabayov, et al, *Nucleic Acids Res.* **2020**, *48*, 12415–12435.

Table of Contents

Hadamard encoded saturation transfer is a promising method capable of measuring enhanced NOE-based correlations from labile protons. Such a method, however, fails when detecting correlations *within* a pool of labile protons by generating artifacts. Here, the origin of these artifacts is elucidated. A way to obtain artifact-free correlations between labile sites as well as between labile and non-labile sites –the extended Hadamard scheme– is then put forward, and its performance corroborated with a series of RNA-based measurements.